Constraints on color-octet fermions from a global parton distribution analysis

Edmond L. Berger,[1] Marco Guzzi,[2] Hung-Liang Lai,[3] Pavel M. Nadolsky,[2] and Fredrick I. Olness[2]

[1]*High Energy Physics Division, Argonne National Laboratory, Argonne, Illinois 60439, USA*

[2]*Department of Physics, Southern Methodist University, Dallas, Texas 75275, USA*

[3]*Taipei Municipal University of Education, Taipei, Taiwan*

(Received 25 October 2010; published 22 December 2010)

We report a parton distribution function analysis of a complete set of hadron scattering data, in which a color-octet fermion (such as a gluino of supersymmetry) is incorporated as an extra parton constituent along with the usual standard model constituents. The data set includes the most up-to-date results from deep inelastic scattering and from jet production in hadron collisions. Another feature is the inclusion in the fit of data from determinations of the strong coupling $\alpha_s(Q)$ at large and small values of the hard scale Q. Our motivation is to determine the extent to which the global parton distribution function analysis may provide constraints on the new fermion, as a function of its mass and $\alpha_s(M_Z)$, independent of assumptions such as the mechanism of gluino decays. Based on this analysis, we find that gluino masses as low as 30 to 50 GeV may be compatible with the current hadronic data. Gluino masses below 15 GeV (25 GeV) are excluded if $\alpha_s(M_Z)$ varies freely (is equal to 0.118). At the outset, stronger constraints had been anticipated from jet production cross sections, but experimental systematic uncertainties, particularly in normalization, reduce the discriminating power of these data.

DOI: 10.1103/PhysRevD.82.114023 PACS numbers: 13.87.−a, 13.85.Qk, 14.80.Ly

I. INTRODUCTION

Heavy color-octet particles are postulated in theories of beyond-the-standard-model (BSM) phenomena, including supersymmetry (SUSY) [1], universal extra dimensions [2], Randall-Sundrum [3], and Little Higgs models [4]. Direct searches for such states are usually guided by aspects of the production and decay dynamics in the particular BSM approach. Analyses of search data have so far produced various bounds on the masses of the states, often conditioned by model-dependent assumptions [5–15]. Different constraints, such as the SUSY gluino mass bounds $m_{\tilde{g}} > 26.9$ GeV [16] and 51 GeV [17] at 95% confidence level (C.L.), are based on the analysis of LEP event shapes in soft-collinear effective theory and other quantum chromodynamics (QCD) resummation formalisms. Constraints such as these may depend on theoretical modeling of nonperturbative hadronization and the matching of hard scattering and resummed contributions, similar to the determination of $\alpha_s(M_Z)$ from LEP data in QCD [18–22]. In a previous publication [23], we examine the possibility that a global analysis of hadron data, within the framework of parton distribution function (PDF) determinations, can be used to derive constraints on the existence and masses of color-octet fermions, independently of other information on such states. Global analysis has discriminating power for several reasons: one is that new colored states modify the evolution with hard scale Q of the strong coupling strength $\alpha_s(Q)$. Second, in perturbative QCD, the coupling of a color-octet fermion to quarks and gluons alters the set of evolution equations that governs the behavior of all parton distribution functions, thus affecting many hadron scattering cross sections. Moreover, production of the color-octet states will affect relevant observables, such as jet rates, whose cross sections are included in the global fits.

The specific case of a gluino from supersymmetry is included as an extra degree of freedom in our earlier work [23]. We refer to the PDFs obtained in that publication as "SUSY PDFs," although our analysis is applicable to a broader class of standard model (SM) extensions. In Ref. [23], a lower bound on the gluino mass $m_{\tilde{g}}$ is obtained in terms of an assumed value of $\alpha_s(M_Z)$ at Z boson mass M_Z. For the then standard model world-average value of $\alpha_s(M_Z) = 0.118$, gluinos lighter than 12 GeV were shown to be disfavored, whereas the lower bound was relaxed to less than 10 GeV (less than 2 GeV) when $\alpha_s(M_Z)$ was increased above 0.120 (0.127).

In this paper, we use new hadron scattering data incorporated in the next-to-leading order (NLO) CT10 general-purpose PDF analysis [24], along with a new approach for incorporating the variation of $\alpha_s(Q)$ into PDF determinations [25], to obtain improved bounds on the mass of a relatively light gluino. The essential new elements are these:

(i) *New Tevatron jet data* [26–28] *and combined DIS data* [29] *from HERA*. In a global QCD analysis, the presence of light gluinos is revealed primarily by modifications of $\alpha_s(M_Z)$, the gluon PDFs, and the charm and bottom quark PDFs, generated radiatively above the respective heavy-quark thresholds. We include the latest hadronic scattering data sensitive to such modifications. The most stringent constraints on the gluon PDF are imposed by electron-proton deep inelastic scattering (DIS) data at $x < 0.1$ and single-inclusive jet production data from the Tevatron $p\bar{p}$ collider at $x \gtrsim 0.1$. The study reported

here incorporates up-to-date information from the combined H1 Collaboration and ZEUS Collaboration data on deep inelastic scattering at HERA-1 [29], as well as single-inclusive jet data from the Tevatron Run-II analyses [26–28]. Hard scattering contributions of massive gluinos, with full dependence on the gluino's mass, are included in the jet production cross sections we use, the only process we examine where these contributions are large enough to be relevant at NLO accuracy.

(ii) *Floating* $\alpha_s(M_Z)$. Our fits are performed by treating $\alpha_s(M_Z)$ at the mass M_Z of the Z boson as a variable parameter of the standard model. We constrain $\alpha_s(M_Z)$ by requiring that the fitted $\alpha_s(Q)$ agree with its direct determinations at low-energy scales ($Q < 10$ GeV) and at $Q = M_Z$, within the quoted uncertainties of these measurements. Virtual gluino contributions result in a slower evolution of the QCD coupling strength $\alpha_s(Q)$ at scales Q above the gluino mass threshold. By including data that constrain α_s at low and high Q scales, we effectively probe for deviations from pure QCD. We find, in particular, that the value of $\alpha_s(M_Z) = 0.123 \pm 0.004$ derived in some analyses of LEP event shapes [20] can be accommodated if gluinos have mass of about 50 GeV.

The remainder of this paper is organized as follows. In Sec. II, we describe the role of new color-octet fermions in a global QCD analysis. The incorporation of data on $\alpha_s(Q)$ within the global fits is discussed in Sec. III, where we also present the values of $\alpha_s(Q)$ at high and low Q used in our fits. Our simultaneous global fit to hadronic scattering data and $\alpha_s(Q)$ is described in Sec. IV, where we also examine the effects of an additional gluino degree of freedom on the PDFs. We present figures that show the relative magnitudes of the PDFs and the variation of their momentum fractions with gluino mass and hard scale.

Section V contains the results of our detailed comparison with data. We present figures that show the variation of the values of χ^2 in the global analyses, as a function of gluino mass, for both floating and fixed $\alpha_s(M_Z)$. Section V also includes the comparison of our calculated cross sections with jet data from the Tevatron collider and a discussion of the systematic uncertainties that limit the constraining power of these data. The sensitivity of jet cross sections at the LHC to the presence of gluinos is examined in Sec. VI. Our conclusions are presented in Sec. VII. The appendices contain an analytic expression for the evolution of the strong coupling $\alpha_s(Q)$ in terms of the SM and SUSY degrees of freedom, expressions for the contributions of massive gluinos to the jet production cross sections, and parton-parton luminosity functions for various combinations of SM partons and gluinos.

Based on our analysis, we conclude that gluino masses as low as 30 to 50 GeV may be compatible with the current hadronic data, depending on the value of $\alpha_s(M_Z)$. For a floating $\alpha_s(M_Z)$, gluinos lighter than 15 GeV are excluded. For an assumed fixed value $\alpha_s(M_Z) = 0.118$, the world-average value used in many phenomenological analyses, gluinos lighter than 25 GeV, are disfavored.

We acknowledge that a gluino as light as ~50 GeV is not typical in phenomenological models of SUSY breaking, nor of the results of experimental direct search analyses based on specific models of SUSY breaking and assumptions about mass relationships among SUSY states [15]. As long as the SUSY neutralino $\tilde{\chi}^0$ is lighter than the gluino, the typical decay process for a light gluino is $\tilde{g} \to q\bar{q}\tilde{\chi}^0$, where q stands for a SM quark. Missing energy would signal the presence of a neutralino. However, for a small mass splitting $m_{\tilde{g}} - m_{\tilde{\chi}^0}$, the gluino's decay into missing energy and soft quark jets would be undetected. The analysis reported here is complementary to other approaches for bounding the gluino mass, and it is in some respects more general in that we make no assumptions about the gluino decay.

Precise determination of $\alpha_s(M_Z)$ and proton PDFs are essential ingredients for obtaining reliable predictions from perturbative QCD calculations. Such calculations are key for the general physics program and for new physics searches at the CERN Large Hadron Collider (LHC) and Fermilab Tevatron collider. As we show here, these ingredients themselves may be affected by non-SM contributions, at all values of the momentum fraction x, as a result of the global interconnections in PDF analyses. The determination of the QCD coupling α_s and of the gluon PDF from the Tevatron or LHC single-inclusive jet data, such as in recent Tevatron Run-2 measurements [26–28,30], may be sensitive to scattering of color-octet fermions in the ways discussed in Sec. VI. As a result of our work, we determine new sets of PDFs that include a relatively light gluino as a hadron constituent.

II. COLOR-OCTET FERMIONS IN A GLOBAL QCD ANALYSIS

Under well-defined conditions, a relatively light strongly-interacting fundamental particle may be treated as a constituent of the colliding hadrons. It will share the momentum of the parent hadron with the standard model quark, antiquark, and gluon partners. The experimental consequences of this picture become evident when the parent hadron is probed at a sufficiently large hard scale. For example, the charm quark c and bottom quark b are treated appropriately as partonic constituents of hadrons when the characteristic energy scale Q exceeds the mass of the heavy quark m_q. Likewise, when Q greatly exceeds the mass of a new strongly-interacting particle, this object must also be incorporated as a hadronic constituent. We refer to Ref. [23] for an exposition of the PDF analysis in which a gluino is included as an additional partonic degree of freedom.

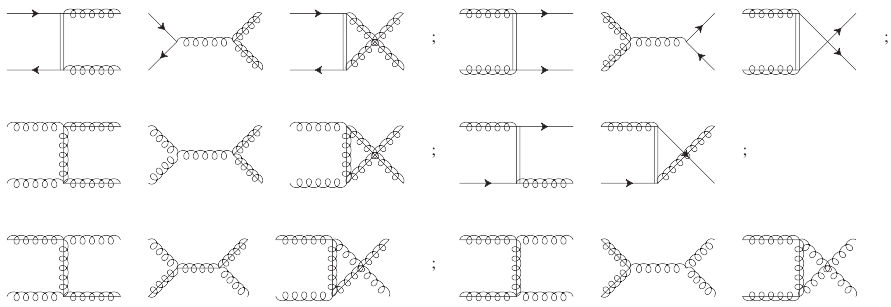

FIG. 1. LO scattering diagrams in inclusive jet production with gluinos in the initial or final state. The double lines stand for the squark exchange contributions that we neglect in our approximation.

As in Ref. [23], we take the gluino as the only colored non-SM degree of freedom that needs to be considered. In some models of SUSY breaking, such as split supersymmetry [31,32], the squarks are much heavier than the gluinos, and therefore could be omitted from our PDF analysis. Moreover, as illustrated in Eq. (A3) of Appendix A, color-octet spin-1/2 fermions have a greater impact on the evolution of the strong coupling α_s than color triplet scalars, such as squarks.[1]

The presence of a light gluino $\tilde{g}$ modifies the PDF global analysis in three ways.

(1) The gluino changes the evolution of the strong coupling strength $\alpha_s(Q)$, as the scale Q is varied. This influence is implemented in our results, and we provide details on the running of $\alpha_s(Q)$ in Appendix A. The constraints on the gluino mass from our global analysis depend significantly on the value of the strong coupling strength $\alpha_s(M_Z)$.

(2) The gluino provides an additional partonic degree of freedom that shares in the nucleon's momentum. It alters the coupled set of Dokshitzer-Gribov-Lipatov-Altarelli-Parisi equations that govern the evolution of the parton distributions,

$$Q^2\frac{d}{dQ^2}\begin{pmatrix}\Sigma(x,Q)\\ g(x,Q)\\ \tilde{g}(x,Q)\end{pmatrix}=\frac{\alpha_s(Q)}{2\pi}\times\int_x^1\frac{dy}{y}\begin{pmatrix}P^{\mathrm{NLO}}_{\Sigma\Sigma}(x/y) & P^{\mathrm{NLO}}_{\Sigma g}(x/y) & P^{\mathrm{LO}}_{\Sigma\tilde{g}}(x/y)\\ P^{\mathrm{NLO}}_{g\Sigma}(x/y) & P^{\mathrm{NLO}}_{gg}(x/y) & P^{\mathrm{LO}}_{g\tilde{g}}(x/y)\\ P^{\mathrm{LO}}_{\tilde{g}\Sigma}(x/y) & P^{\mathrm{LO}}_{\tilde{g}g}(x/y) & P^{\mathrm{LO}}_{\tilde{g}\tilde{g}}(x/y)\end{pmatrix}\begin{pmatrix}\Sigma(y,Q)\\ g(y,Q)\\ \tilde{g}(y,Q)\end{pmatrix};$$
$$\Sigma(x,Q)=\sum_{i=u,d,s,\ldots}(q_i(x,Q)+\bar{q}_i(x,Q)). \tag{1}$$

Here $\Sigma(x,Q)$, $g(x,Q)$, and $\tilde{g}(x,Q)$ are the singlet quark, gluon, and gluino distributions, respectively; $q_i(x,Q)$ and $\bar{q}_i(x,Q)$ are the quark and antiquark distributions for a flavor i. The previous analysis [23] shows that the gluino's contribution is small in the momentum fraction range $x>10^{-5}$, $\tilde{g}(x,Q)\ll g(x,Q)$, and $\tilde{g}(x,Q)\ll q(x,Q)$. NLO variations in the relevant SUSY cross sections are small and comparable in size to variations associated with next-to-next-to-leading order (NNLO) SM contributions. Therefore, the leading-order (LO) approximation for the splitting functions and hard scattering amplitudes of SUSY terms is numerically adequate, when combined with NLO expressions for SM contributions.

(3) At energies above its mass threshold, a color-octet fermion contributes to hard scattering processes as an incident parton and/or as a produced particle. However, as argued in Ref. [23], in the absence of light squarks, gluino hard scattering contributions to DIS and Drell-Yan process are of next-to-next-to-leading order and negligible in the current study. At the same time, the hard scattering gluino terms contribute at the LO in single-inclusive jet production, so that it is essential that we include the gluino in the corresponding hard scattering matrix elements of jet cross sections.

The $2\to 2$ hard scattering contributions with two gluinos in the initial or final states are illustrated in Fig. 1. We assume that the masses of the squarks are large enough that diagrams containing a squark propagator are negligible. The remaining SUSY diagrams can be evaluated in the the S-ACOT factorization scheme [34,35], in order to simplify treatment of the gluino mass dependence. In this scheme, gluino mass terms are retained in diagrams with two final-state gluinos in the subprocesses $gg\to\tilde{g}\,\tilde{g}$ and $q\bar{q}\to\tilde{g}\,\tilde{g}$. Explicit scattering amplitudes in these

[1]While bottom squarks ($\tilde{b}$) can be relatively light in some models [33], their contribution to DIS and other relevant cross sections can be neglected, cf. Ref. [23].

channels are documented in Eqs. (B2) and (B3) of Appendix B. Massless amplitudes are used for the remaining $2 \to 2$ hard scattering subprocesses, in which one or two gluinos are present in the initial state, and whose contributions are proportional to the gluino PDF $\tilde{g}(x, Q)$. This arrangement captures the full gluino mass dependence, while including the mass terms only in the essential scattering amplitudes.

III. QCD COUPLING STRENGTH AS A FITTING PARAMETER

Since the range of $m_{\tilde{g}}$ values allowed by the global fits depends strongly on the assumed value of $\alpha_s(M_Z)$, we do a simultaneous fit to hadronic data and to data on $\alpha_s(Q)$ in this work. A judicious choice is required therefore of the set of data on $\alpha_s(Q)$.

Our approach is to fit the global set of data using $\alpha_s(Q)$ as a floating parameter, constraining it with additional data on $\alpha_s(Q)$ measurements at $Q < 10$ GeV (i.e., in the range where gluino contributions are excluded by the previous analysis), and at $Q = M_Z$ (in e^+e^- hadroproduction at LEP). This approach is similar to the floating $\alpha_s(M_Z)$ fit in Ref. [25]. However, we constrain $\alpha_s(Q)$ at two distinct Q values, to probe for deviations of its running from the SM prediction.

A. Low-energy constraints

The QCD coupling constraint at low $Q = 5$ GeV,

$$\alpha_s(Q = 5\ \text{GeV}) = 0.213 \pm 0.002, \tag{2}$$

is obtained as a weighted average of three precise determinations of α_s at comparable energies:

$$\alpha_s(Q = 5\ \text{GeV}) = 0.219 \pm 0.006 \quad \text{from } \tau \text{ decays}, \tag{3}$$

$$\alpha_s(Q = 5\ \text{GeV}) = 0.214 \pm 0.003 \quad \text{from heavy quarkonia}, \tag{4}$$

$$\alpha_s(Q = 5\ \text{GeV}) = 0.209 \pm 0.004 \ \text{from lattice QCD}. \tag{5}$$

These values are reconstructed by QCD evolution to the common scale $Q = 5$ GeV of the published α_s values provided at different energy scales,

$$(\alpha_s)_\tau = 0.330 \pm 0.014 \quad \text{at } m_\tau = 1.77\ \text{GeV}, \tag{6}$$

$$(\alpha_s)_{Q\bar{Q}} = 0.1923 \pm 0.0024 \quad \text{at } M_{Q\bar{Q}} = 7.5\ \text{GeV}, \tag{7}$$

$$(\alpha_s)_{\text{lattice}} = 0.1170 \pm 0.0012 \quad \text{at } M_Z = 91.18\ \text{GeV}. \tag{8}$$

The value of $(\alpha_s)_\tau$ is determined from measurements of τ decays [36], $(\alpha_s)_{Q\bar{Q}}$ comes from heavy-quarkonium decays [37], and $(\alpha_s)_{\text{lattice}}$ is obtained from lattice computations [37].

The τ decay and heavy-quarkonium determinations of α_s can be reasonably assumed to be independent of gluino effects. Even if very light gluinos (≈ 10 GeV) were present, the value of α_s in these measurements would not be affected. The lattice QCD value $(\alpha_s)_{\text{lattice}}$ is also determined at $Q < 10$ GeV from the energy levels of heavy quarkonia [37], and then evolved by the authors to $Q = M_Z$ assuming the SM β function. We reconstruct the "directly measured" lattice QCD value at $Q = 5$ GeV (independent of the gluino effects) by backward SM evolution. We then combine the lattice QCD value with the other two low-Q measurements, evolved to the same scale using the SM β function, to obtain a composite data input to the fit.

B. Z pole constraints

If $m_{\tilde{g}} < M_Z$, the value of $\alpha_s(M_Z)$ extracted from the LEP e^+e^- hadroproduction data could differ from the value obtained from SM fits. On the other hand, various determinations of $\alpha_s(M_Z)$ from Z boson width and hadronic event shapes [18–22,38] show no obvious need for BSM contributions. Thus, if gluinos are lighter than Z bosons, their contributions to the LEP observables are of the order of theoretical uncertainties from other sources. Notably related to assumptions about nonperturbative hadronization in LEP observables, these uncertainties remain substantial and produce central values of $\alpha_s(M_Z)$ ranging from 0.1135 [21,22] to 0.1224 [20]. To deal with this issue of choice, one solution is to include available values of $\alpha_s(M_Z)$ derived from the Z width and/or event shape measurements, assuming that gluino contributions for these measurements are comparable with the current experimental plus theoretical uncertainties.

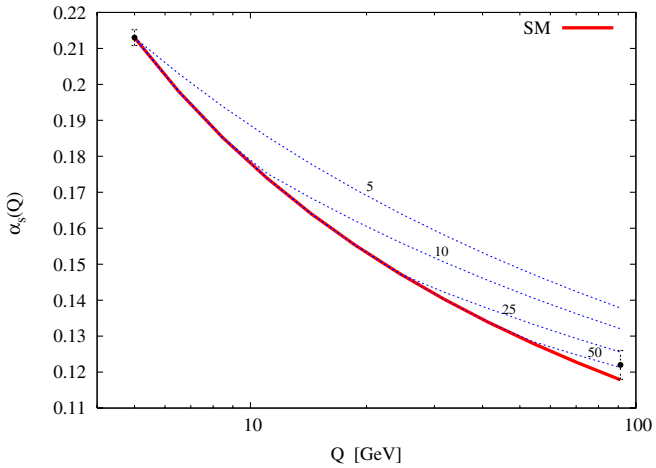

FIG. 2 (color online). Running of the strong coupling as a function of the scale Q. The red solid line represents the SM evolution, while the dashed lines are plotted for $m_{\tilde{g}} = 50, 25, 10, 5$ GeV. The points with the error bands represent the low-Q and high-Q constraints, given in Eqs. (2) and (9), respectively.

Absent a gluino lighter than the Z boson (i.e., if only SM particles contribute at $Q < M_Z$), NLO evolution of the composite low-Q value in Eq. (2) to the Z pole results in $\alpha_s(M_Z)$ close to 0.118. Global analysis of hadronic scattering alone also leads to a preferred value $\alpha_s(M_Z) = 0.118 \pm 0.005$ at 90% C.L., cf. recent CTEQ fits [25].

If the gluino is lighter than M_Z, the resulting evolved value at $Q = M_Z$ is higher. For example, the evolved $\alpha_s(M_Z)$ is 0.126 or 0.121, if $m_{\tilde{g}}$ is 20 or 50 GeV. This variation is illustrated in Fig. 2, showing the dependence of $\alpha_s(Q)$ on the scale Q in the absence of light gluinos (solid line) and with gluinos of mass $m_{\tilde{g}} = 50$, 25, 10, and 5 GeV. In the figure, we show the low-Q constraint (the left data point), as well as one of available constraints at the Z pole, $\alpha_s(M_Z) = 0.123 \pm 0.004$ [20]. As seen in the figure, a light gluino with a mass of $m_{\tilde{g}} = 10$ GeV cannot simultaneously accommodate the low-Q and high-Q constraints. On the other hand, gluinos with mass about 50 GeV are compatible with both constraints, and are even preferred if the high-Q constraint on α_s is larger than 0.118.

To illustrate typical possibilities, we therefore present two kinds of fits in this paper: one in which a fixed value of $\alpha_s(M_Z) = 0.118$ is assumed, and the other in which $\alpha_s(M_Z)$ varies and is constrained by an assumed high-Q data point,

$$\alpha_s(M_Z) = 0.123 \pm 0.004, \tag{9}$$

compatible with [20].

C. Log-likelihood function for coupling strength constraints

With the additional constraints on the running coupling, the total log-likelihood function $\chi^2_{\rm tot}$ is

$$\chi^2_{\rm tot} = \chi^2_{\rm h.s.} + \chi^2_{\alpha_s}, \tag{10}$$

where $\chi^2_{\rm h.s.}$ is the χ^2 contribution of the hadron scattering (h.s.) experiments, i.e., DIS, vector boson production, and jet production; $\chi^2_{\alpha_s}$ is the contribution from the direct constraints on α_s:

$$\chi^2_{\alpha_s} = \lambda \sum_{i=1}^{N_{\alpha_s}} \left(\frac{\alpha_s^{(i)}|_{\rm exp} - \alpha_s^{(i)}|_{\rm th}}{\delta\alpha_s^{(i)}|_{\rm exp}} \right)^2. \tag{11}$$

In this equation, N_{α_s} is the number of data points constraining α_s; $N_{\alpha_s} = 2$ in our case. $\alpha_s^{(i)}|_{\rm exp}$ and $\delta\alpha_s^{(i)}|_{\rm exp}$ are the central value and error of the experimental measurements in Eqs. (2) and (9); $\alpha_s^{(i)}|_{\rm th}$ are the respective two-loop theoretical values. We assume that an increase in χ^2 by 100 units above the best-fit value corresponds to approximately 90% C.L. error, in accordance with the convention of the previous CTEQ6 analysis [39] and 2004 gluino study [23]. To match this convention, the α_s contribution $\chi^2_{\alpha_s}$ is included with a factor $\lambda = 37.7$, so that a deviation of $\alpha_s^{(i)}|_{\rm th}$ by $1.6\delta\alpha_s^{(i)}|_{\rm exp}$ (90% C.L.) corresponds to $\Delta\chi^2_{\alpha_s} \approx 100$.

IV. GLOBAL FITS

In this section we describe our simultaneous global fit to hadronic scattering data and $\alpha_s(Q)$, and we examine the effects of an additional gluino degree of freedom on the PDFs.

Our SUSY fits include the same set of data as the latest CT10 fit of parton distributions [24]. A total of 2753 data points from 35 experiments is included. Besides the data studied in the previous CTEQ6.6 analysis [40], the new analysis includes the combined DIS data from HERA-1 [29] and single-inclusive jet data from the Tevatron Run-2 analyses [26–28]. The new data provide important constraints on the gluon PDF, the parton density that is most affected by the gluinos. The charm and bottom PDFs are also affected, since they are generated by DGLAP evolution from the gluon PDF above the initial scale $Q_0 = m_c = 1.3$ GeV.

The ratios of the best-fit gluon and charm PDFs in the SUSY sets to their counterparts in the standard model CT10 set, $f_{\rm SUSY}(x, Q)/f_{\rm CT10}(x, Q)$, are shown as dashed curves in Figs. 3 and 4, at $Q = 2$ and 85 GeV, for two values of the gluino mass, $m_{\tilde{g}} = 20$ and 50 GeV. The normalized CT10 uncertainty bands are shown also, defined as

$$\frac{f_{\rm CT10}(x, Q) \pm \delta_{\pm} f_{\rm CT10}(x, Q)}{f_{\rm CT10}(x, Q)} \tag{12}$$

in terms of asymmetric PDF uncertainties $\delta_{\pm} f_{\rm CT10}(x, Q)$ [24,41]. Figure 3 pertains to fits with a floating $\alpha_s(M_Z)$, whereas Fig. 4 is based on a fixed $\alpha_s(M_Z) = 0.118$.

If $\alpha_s(M_Z)$ varies (Fig. 3), modifications in the gluon distribution are moderate at most. Some differences with the CT10 predictions are observed at large x, notably in the range $x > 0.01$ in $g(x, Q)$ at $Q = 85$ GeV and in $c(x, Q)$ at $Q = 2$ GeV. The difference is larger for a lighter gluino with $m_{\tilde{g}} = 20$ GeV. Other PDFs exhibit smaller differences, all contained in the standard model uncertainty band.

For a fixed $\alpha_s(M_Z) = 0.118$ (Fig. 4), the differences with CT10 are substantial. At $Q = 2$ GeV, the SUSY PDFs lie outside of CT10 error bands for x as low as 10^{-3}. At $Q = 85$ GeV, the difference persists at $x > 0.01 - 0.05$. Large differences between the SUSY and CT10 PDF's in the case of a fixed strong coupling are attributed to sizable deviations from SM running of α_s and compensating adjustments in $g(x, Q)$ observed for relatively light gluinos; cf. Figs. 12b and 5 in Ref. [23].

The effect of the gluino on the standard model quark and gluon PDFs can be significant, even if $m_{\tilde{g}}$ is large compared to m_c and m_b.[2] Because the gluino is an active

[2]We use $m_c = 1.3$ GeV and $m_b = 4.5$ GeV. The up, down, and strange quark masses $\{m_u, m_d, m_s\}$ do not play a role in the evolution, as they are less than the initial evolution scale $Q_0 = 1.3$ GeV.

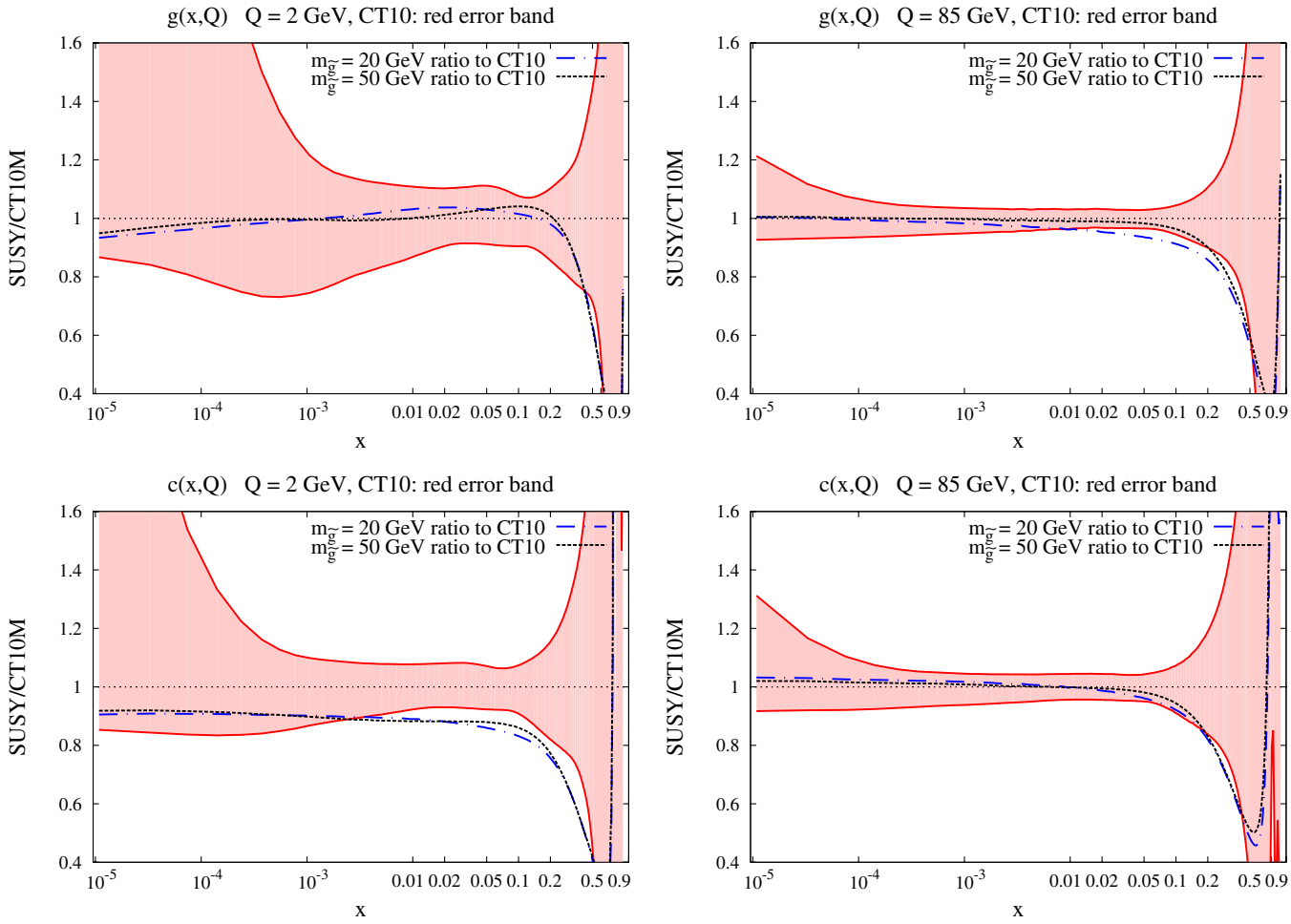

FIG. 3 (color online). Ratios of $g(x, Q)$ (upper row) and $c(x, Q)$ (lower row) distributions in SUSY fits with floating $\alpha_s(M_Z)$ and the CT10 fit at $Q = 2$ GeV (left) and $Q = 85$ GeV (right), for the gluino mass $m_{\tilde{g}}$ of 20 and 50 GeV.

constituent of the proton, it carries a finite momentum fraction, taken from the other non-SUSY partons, primarily the gluon. This feature is evident in Table I where we display the partonic momentum fractions for gluino masses $m_{\tilde{g}} = \{20, 50, 100\}$ GeV.

Gluinos draw most of their momentum fraction from the gluon, since the primary coupling is via the process $g \to \tilde{g}\,\tilde{g}$. The influence on the quarks is a second-order effect transmitted through the gluon. At $Q = 100$ GeV, the momentum fraction of the lighter gluinos ($m_{\tilde{g}} \sim 20$ GeV) is comparable to that of the strange quark, even though the gluino mass is an order of magnitude larger. For $m_{\tilde{g}} \sim 50$ GeV, the momentum fraction of the gluino is comparable to that of the bottom quark. The magnified impact of the gluino on the QCD evolution, compared to the usual quark flavors, can be understood from a comparison of the $g \to \tilde{g}$ splitting kernel,

$$P_{g\to\tilde{g}}(x) = 3[(1-x)^2 + x^2], \tag{13}$$

with the usual gluon-quark splitting function

$$P_{g\to q}(x) = \tfrac{1}{2}[(1-x)^2 + x^2]. \tag{14}$$

The effect of the gluino as a hadronic constituent in the QCD evolution is thus equivalent to that of 6 quark flavors, $P_{g\to\tilde{g}} = 6P_{g\to q}$.

As an illustration of the relative magnitude of the gluino PDF, Fig. 5 displays PDFs for various parton flavors as a function of x for our $m_{\tilde{g}} = 50$ GeV PDF set and a hard scale of $Q = 100$ GeV. At $x > 0.001$, the gluino PDF is about equal to the bottom quark PDF, the smallest of the quark PDFs. For smaller x, it grows in magnitude and catches up with the other quark PDFs at $x = 10^{-5}$, as a consequence of its faster DGLAP evolution. Parton-parton luminosities dependent on the gluino PDF, useful for computations of cross sections, are plotted in Appendix C.

V. COMPARISON OF THEORY AND DATA

In this section, we show the results of our global fits, the constraints we obtain on the mass of a gluino, and the impact of a gluino degree of freedom on the analysis of jet data.

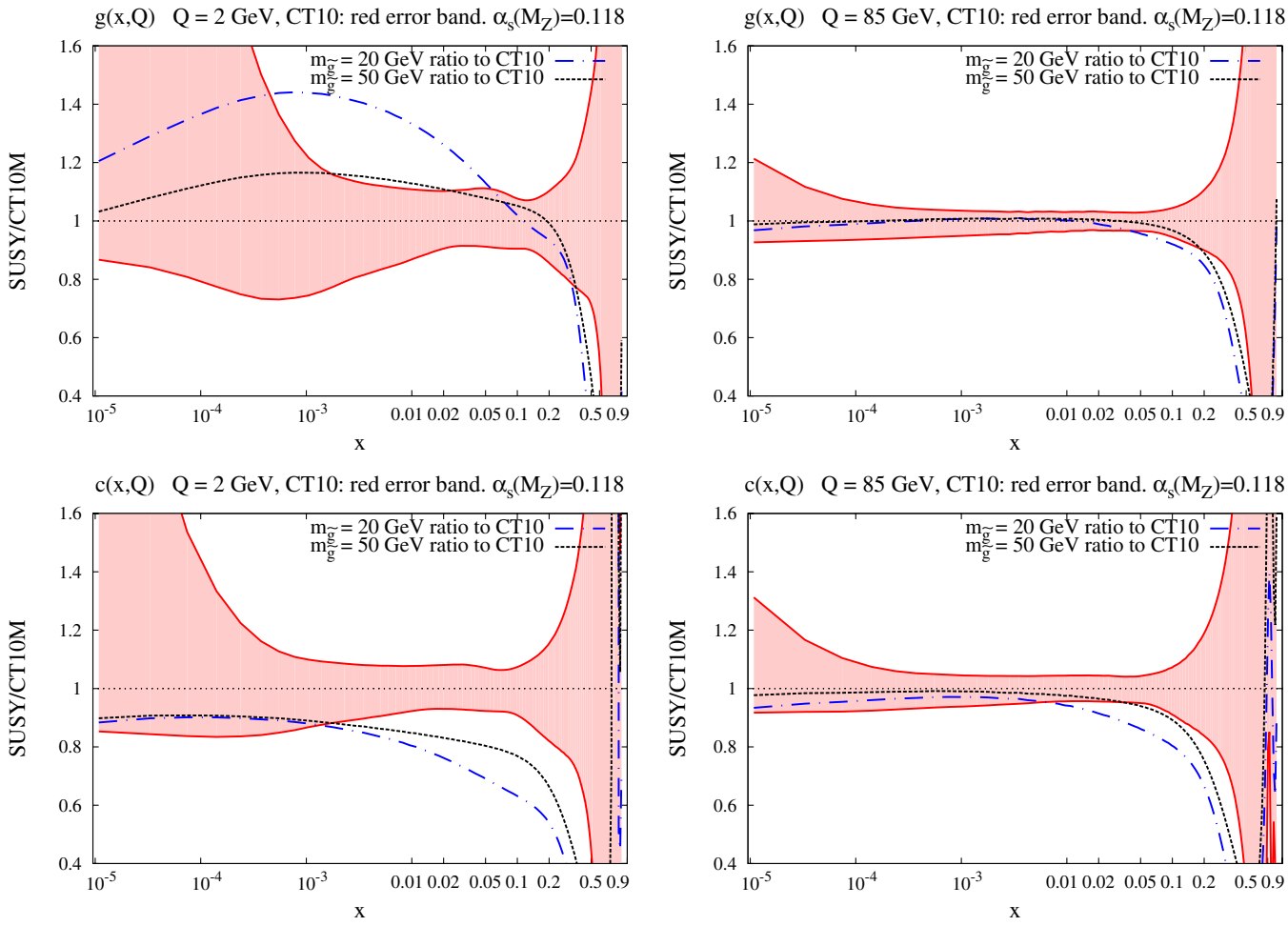

FIG. 4 (color online). Same as Fig. 3, but for a fixed $\alpha_s(M_Z) = 0.118$.

The figures in the previous section show that the SM +SUSY PDFs disagree with CT10 PDFs if gluinos are lighter than 20 GeV, indicating that the SM+SUSY PDFs for these gluino masses cannot describe the global hadronic data well. Gluinos with somewhat larger masses can be accommodated, or may be slightly preferred to the pure SM case, depending on the value of $\alpha_s(M_Z)$. These points are illustrated in a different way by the summary of values of χ^2 in Table II, for $m_{\tilde{g}} = 10$, 20, and 50 GeV, as well as for the standard model case (equivalent to $m_{\tilde{g}} = \infty$). The table shows the log-likelihood values $\chi^2_{\text{h.s.}}$ and χ^2_{tot}, without and with the imposition of α_s constraints, as defined in Eqs. (10) and (11); as well as χ^2 per number of data points for HERA-1 DIS [29] and Tevatron Run-1 and Run-2 single-inclusive jet cross sections [26–28,42,43]. In the fit with a floating α_s, the best-fit $\alpha_s(M_Z)$ is also shown. A comparison of the upper and lower halves of the table shows that the relation between χ^2 and $m_{\tilde{g}}$ depends on whether $\alpha_s(M_Z)$ is fixed or floating.

TABLE I. Momentum fraction $F_i = \int_0^1 dx x f_i(x, Q)$ for each partonic flavor i at scale $Q = 100$ GeV. Momentum fractions for $\{\bar{s}, \bar{c}, \bar{b}\}$ are not shown and must be included to satisfy the sum rule.

Momentum fractions for $Q = 100$ GeV in percent									
$m_{\tilde{g}}$ [GeV]	$\tilde{g}$	d	$\bar{u}$	g	u	d	s	c	b
20	2.8	3.9	3.4	44.3	21.8	11.4	3.0	1.8	1.2
50	1.2	3.9	3.4	45.8	21.8	11.4	3.1	1.9	1.2
100	0	3.9	3.4	47.1	21.7	11.4	3.0	1.9	1.2

Fixed $\alpha_s(M_Z)$. In a fit with a fixed $\alpha_s(M_Z)$, only constraints from the hadronic data, associated with the term $\chi^2_{\text{h.s.}}$ (and not with the total χ^2_{tot}) play a meaningful role. The upper half of Table II shows χ^2 values from a fit with fixed $\alpha_s(M_Z) = 0.118$.[3] In this case, the gluino's effect of slowing the evolution of $\alpha_s(Q)$ from $Q = M_Z$ to $Q = 5$ GeV runs into strong disagreement with the low-Q

[3]This value, compatible with the current world average, is about 1σ below $\alpha_s(M_Z) = 0.123 \pm 0.004$; hence, the SM fit with this $\alpha_s(M_Z)$ value has a higher χ^2_{tot} (in the last line of the upper table) than a fit with a floating $\alpha_s(M_Z)$ (in the last line of the lower table).

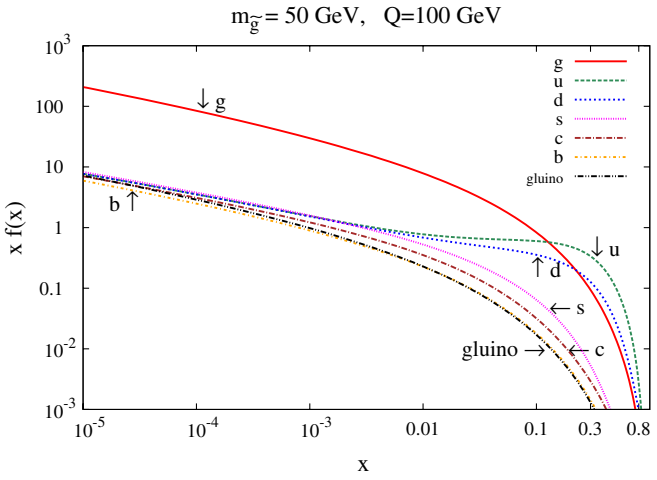

FIG. 5 (color online). PDFs for various flavors at $Q = 100$ GeV, for $m_{\tilde{g}} = 50$ GeV.

constraint; $\chi^2_{\rm tot}$ grows quickly as $m_{\tilde{g}}$ decreases, corresponding to a difference of many standard deviations between the measured and predicted α_s values at $Q = 5$ GeV. More importantly, the hadronic data by themselves disfavor very light gluinos, with $m_{\tilde{g}} = 25$ GeV or less excluded according to the criterion $\Delta\chi^2 \equiv \chi^2_{\rm SUSY}(m_{\tilde{g}}) - \chi^2_{\rm CT10} < 100$ applied to $\chi^2_{\rm h.s.}$.

Floating $\alpha_s(M_Z)$. The values in the lower half of Table II are for SM+SUSY fits with a variable $\alpha_s(M_Z)$. In this case, the constraints from both the hadronic scattering and direct measurements of $\alpha_s(M_Z)$ are relevant. The most meaningful log-likelihood term is $\chi^2_{\rm tot} = \chi^2_{\rm h.s.} + \chi^2_{\alpha_s}$. If $\alpha_s(M_Z)$ varies, the hadronic scattering data on their own, including the HERA-1 and Tevatron jet data sets, are compatible with practically any gluino mass. The contribution to χ^2 from the hadron scattering experiments, $\chi^2_{\rm h.s.}$, stays approximately the same as in the SM case, or improves slightly, as gluinos with masses of 10, 20, and 50 GeV are introduced.

This agreement with the hadronic scattering data, hardly affected by the gluino mass, results from compensation between modifications in the shape of the gluon PDF and an increase in the preferred $\alpha_s(M_Z)$, which grows from 0.118 in the SM case to 0.132 for $m_{\tilde{g}} = 10$ GeV. In contrast, the total likelihood function for the fit to the hadronic scattering data and α_s values, introduced as $\chi^2_{\rm tot}$ in Eq. (10), varies considerably as a function of the gluino mass. Our assumed high-Q constraint of $\alpha_s(M_Z) = 0.123 \pm 0.004$ is slightly higher than $\alpha_s(M_Z) = 0.118$ obtained by the SM evolution from $\alpha_s(Q = 5\ {\rm GeV}) = 0.213 \pm 0.002$ in Eq. (2). This enhanced value of $\alpha_s(M_Z)$ would favor a slower QCD evolution above the gluino mass threshold at about 50 GeV, cf. Figure 2. Consequently, $\chi^2_{\rm tot}$ is smaller at $m_{\tilde{g}} = 50$ GeV than in the SM case, with the difference dependent on the choice of the high-Q value of $\alpha_s(M_Z)$. Specifically, we observe that $\chi^2_{\rm SUSY}(m_{\tilde{g}}) - \chi^2_{\rm CT10}$ can be as small as -50, if we take $\alpha_s(M_Z) = 0.123 \pm 0.004$, but this difference decreases if a smaller $\alpha_s(M_Z)$ is used for the high-Q constraint. For lower gluino masses of 10 or 20 GeV, $\alpha_s(M_Z)$ increases and eventually is incompatible with the direct constraints.

A. $\Delta\chi^2$ as a function of gluino mass

The behavior of $\Delta\chi^2$ in the whole range of gluino masses is illustrated by Fig. 6 for a fixed $\alpha_s(M_Z) = 0.118$, and by Fig. 7 for a floating $\alpha_s(M_Z)$. The quantitative likelihood of a given mass $m_{\tilde{g}}$ is specified by $\Delta\chi^2 = \chi^2(m_{\tilde{g}}) - \chi^2_{\rm CT10}$, the difference from the χ^2 value obtained in the CT10 SM fit. Values of $\Delta\chi^2$ in excess of 100 units disfavor an assumed $m_{\tilde{g}}$ at about 90% C.L. (Refs. [23,39]), while a negative $\Delta\chi^2$ indicates a preference for this $m_{\tilde{g}}$. Variations in $\Delta\chi^2$ with a magnitude below 100 units can result from a variety of sources and are generally viewed as not significant enough to warrant strong conclusions.

In Fig. 6, two curves are shown for $\Delta\chi^2_{\rm h.s.}$, the difference between the log-likelihoods in the fits performed in the

TABLE II. χ^2 values in the global analyses with a floating and fixed $\alpha_s(M_Z)$, for various gluino mass values.

SUSY analysis with a fixed $\alpha_s(M_Z) = 0.118$					
$m_{\tilde{g}}$ [GeV]	$\chi^2_{\rm h.s.}$	$\chi^2_{\rm tot}$	χ^2/npt: HERA-1	χ^2/npt: jet prod.	$\alpha_s(M_Z)$
10	3154	12550	1.31	1.24	0.118
20	3030	7882	1.24	1.19	0.118
50	2923	3788	1.18	1.10	0.118
∞	2918	3004	1.16	1.09	0.118
SUSY analysis with a floating $\alpha_s(M_Z)$					
$m_{\tilde{g}}$ [GeV]	$\chi^2_{\rm h.s.}$	$\chi^2_{\rm tot}$	χ^2/npt: HERA-1	χ^2/npt: jet prod.	$\alpha_s(M_Z)$
10	2892	3124	1.14	1.06	0.132
20	2897	2958	1.15	1.06	0.127
50	2896	2901	1.15	1.03	0.121
∞	2918	2960	1.16	1.09	0.118

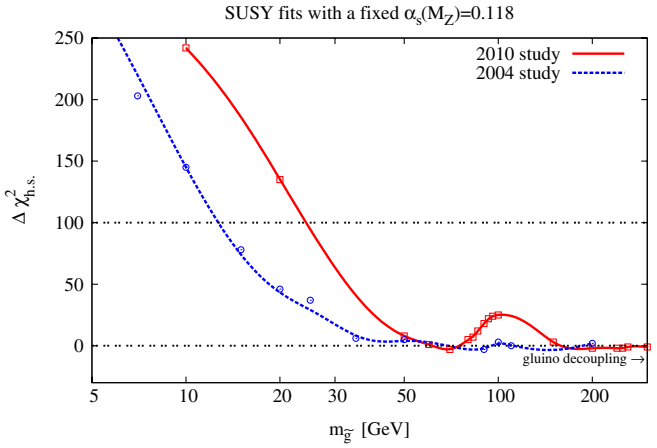

FIG. 6 (color online). Values of $\Delta\chi^2_{\rm h.s.}$ vs $m_{\tilde{g}}$ are shown for a fixed value of $\alpha_s(M_Z) = 0.118$ for the 2004 study (blue dashed line) and our new one (red solid line).

SM+SUSY and SM scenarios for $\alpha_s(M_Z) = 0.118$. Here $\Delta\chi^2_{\rm h.s.}$ is computed from the hadronic scattering contribution only, $\chi^2_{\rm h.s.}$. The blue (dashed) curve represents the 2004 analysis [23]. The red (solid) curve is obtained in the present study, resulting in a tighter lower bound on $m_{\tilde{g}}$. The left branch of the 2010 curve intercepts the $\Delta\chi^2_{\rm h.s.} = 100$ line at $m_{\tilde{g}} \approx 25$ GeV. The 2004 curve allows for 15 GeV gluinos and has a broader valley with respect to the 2010 one. This figure shows the improvements in the constraints from the present study, reflecting the inclusion of the latest precise data and technical advances in the the CTEQ analysis since the 2004 publication, including treatment of correlated systematic uncertainties and normalization uncertainties.

Figure 7 illustrates the fits with a variable $\alpha_s(M_Z)$. Two curves are shown for $\Delta\chi^2_{\rm tot}$, the difference between the log-likelihoods in the fits performed in the SM+SUSY and SM scenarios in 2004 (blue dashed line) and 2010 (red solid line). Best-fit values of $\alpha_s(M_Z)$ for some gluino masses are indicated by numerical labels near each curve. In this figure, $\Delta\chi^2_{\rm tot}$ is computed from the total function $\chi^2_{\rm tot}$. It includes the direct constraints on $\alpha_s(Q)$ in the current study and does not include the α_s constraint in the 2004 fit.

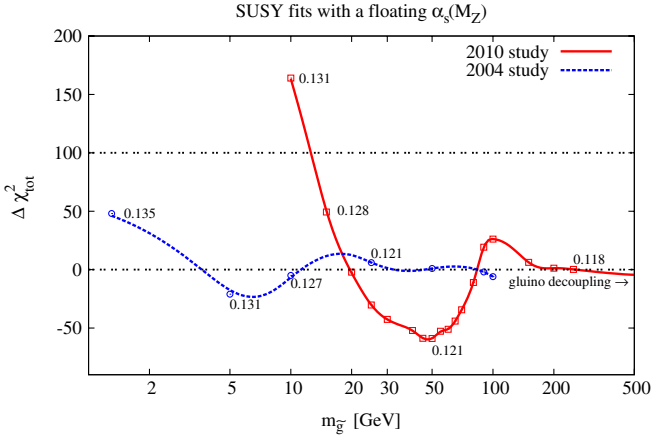

FIG. 7 (color online). Values of $\Delta\chi^2_{\rm tot}$ vs $m_{\tilde{g}}$ are shown for varying values of $\alpha_s(M_Z)$ for the 2004 study (blue dashed) and our new one (red solid).

The figure emphasizes our earlier observation that the direct α_s constraints improve the constraining power of the global analysis. At $m_{\tilde{g}} \to \infty$, the fit converges to the pure QCD value and $\alpha_s(M_Z) \approx 0.119$. According to the $\Delta\chi^2 \leq 100$ test, gluinos lighter than 15 GeV are disfavored for all $\alpha_s(M_Z)$. Gluinos in the mass range 15 to 50 GeV are allowed if $\alpha_s(M_Z)$ takes a value in the range 0.121 to 0.131. Gluinos heavier than 50 GeV are allowed for practically any $\alpha_s(M_Z)$ value. By contrast, the 2004 curve exhibits only a shallow minimum around 5 to 6 GeV, and it is relatively flat as compared to the 2010 curve. The 2004 curve does not establish pronounced lower bounds on $m_{\tilde{g}}$, for a free $\alpha_s(M_Z)$.

The 2010 curve in Fig. 7 exhibits an intriguing minimum for a gluino of about 50 GeV, corresponding to $\alpha_s(M_Z)$ of 0.121. Other that noting it, we choose not to base conclusions on this minimum for two reasons. First, from the point of view of the fit itself, given its initial inputs, we adhere to statement that only values of $|\Delta\chi^2|$ in excess of 100 units are considered significant. Second, the depth of this minimum is a reflection of the value of the input constraint $\alpha_s(M_Z) = 0.123 \pm 0.004$. The dip grows deeper (becomes more shallow) if a larger (smaller) value of the direct constraint is taken at M_Z. For example, gluinos with mass 50 GeV would be disfavored if the direct constraint $\alpha_s(M_Z) < 0.118$ were taken, compatible with some existing analyses of LEP data in pure QCD [21,22]. Stronger conclusions on $m_{\tilde{g}}$ await an independent reduction in the uncertainties on $\alpha_s(M_Z)$.

B. Comparison with Tevatron jet cross sections

Table II indicates that the hadronic scattering data, including the combined HERA-1 and Tevatron jet cross sections, may still allow contributions from fairly light gluinos. This observation is somewhat counterintuitive with regard to the precise Tevatron jet cross sections, which could be expected to be sensitive to non-SM contributions in the strong interaction sector. SUSY degrees of freedom introduce new subprocesses in the jet cross sections, such as $gg \to \tilde{g}\,\tilde{g}$ and $q\bar{q} \to \tilde{g}\,\tilde{g}$. The change in $\alpha_s(Q)$ and the alteration of the gluon and quark PDFs also influence the jet rate. However, jet cross section measurements are affected by systematic effects that dominate over statistical uncertainties, notably by the uncertainty on jet energy scale and jet energy resolution. Correlated systematic shifts in the Tevatron jet data must be taken into account when comparisons are made to theory predictions [44]. In our study, systematic uncertainties in the jet data limit the strength of our conclusions.

These observations are illustrated by plots of the CDF Run-2 and D0 Run-2 data vs theory in Figs. 8 and 9. Our results are computed with a floating α_s. As reference values, we use SM cross sections computed with the CT10 PDFs. Differences from the SM cross section are presented as

$$(\sigma_i - \sigma_{\mathrm{CT10}})/\sigma_{\mathrm{CT10}}, \tag{15}$$

where σ_i are the SM+SUSY cross sections computed for gluino masses of 10, 20, and 50 GeV. The values of the jet transverse momentum p_T are displayed along the horizontal axis. Two bins in the rapidity variable y are shown for each experiment; the behavior in the rest of the bins is similar.

The lower (red) error bars represent the unshifted data. The upper (blue) error bars show the data that are shifted by their systematic uncertainty so as to maximize the agreement with theory for $m_{\tilde{g}} = 10$ GeV. Without the correlated shifts, the data would disfavor the light gluinos with a mass of 10 GeV. The perspective changes significantly if systematic shifts are allowed: the line representing

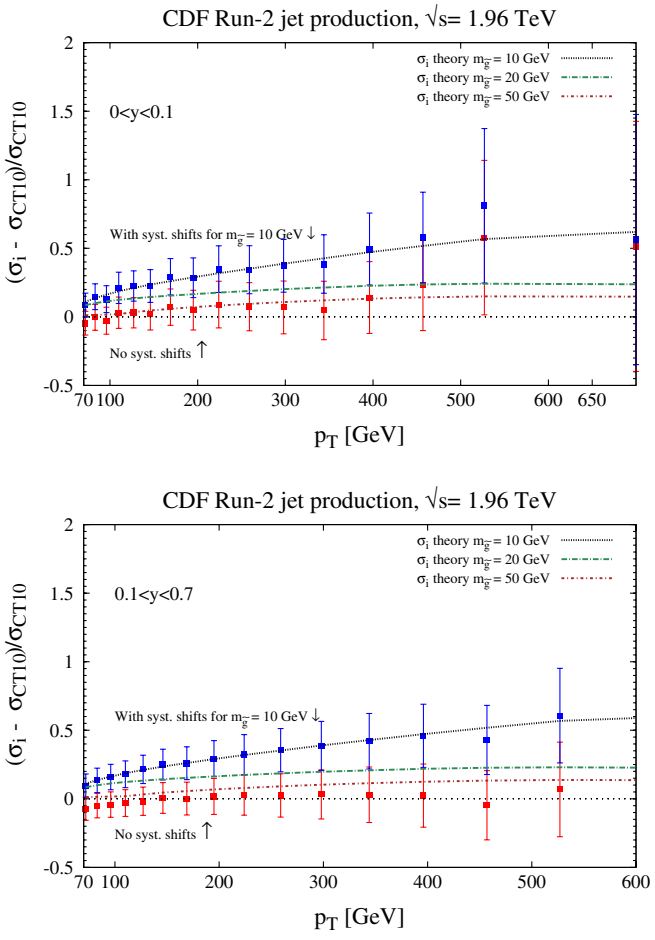

FIG. 8 (color online). Comparison of theoretical predictions for single-inclusive jet cross sections with data from CDF Run-2 for two bins in jet rapidity y.

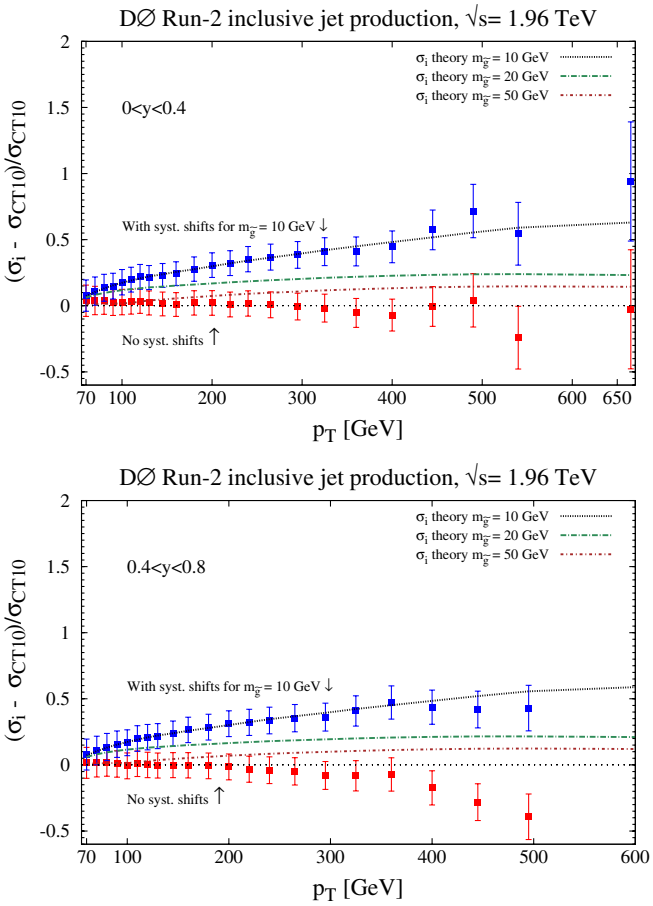

FIG. 9 (color online). Same as Fig. 8, for two bins in jet rapidity y in the D0 Run-2 jet cross section measurement.

$m_{\tilde{g}} = 10$ GeV now lies completely inside the error bars. Similarly, if $m_{\tilde{g}}$ is equal to 20 or 50 GeV, the effective shifts of the data change to achieve acceptable agreement with the theory curve for this mass.[4]

The systematic uncertainties make it difficult to disfavor the light gluinos solely on the basis of the Tevatron Run-2 jet data. The figures show that the gluino contributions affect the whole p_T range, as a result of the momentum sum rule and other connections between the PDFs of different flavors and at different (x, Q) values. Modifications in the jet cross sections due to "new physics" associated with the gluinos cannot be isolated to a specific p_T interval, contrary to the assumptions made in some experimental studies of jet cross sections [30].

VI. CROSS SECTIONS AT THE LHC

The possible existence of color-octet fermions with masses in the range 30 to 100 GeV, allowed by hadronic

[4]The extent of plausible systematic shifts is determined by matrices of correlated systematic errors, provided by both Tevatron collaborations and implemented in the CT09 [44] and CT10 analyses [25].

data according to our analysis, raises the prospects for their detection in the extended range of transverse momenta at the LHC. As explained in early sections of this paper, these new fermions modify QCD inputs, primarily the QCD coupling $\alpha_s(M_Z)$ and the gluon and sea-quark PDFs. Precise studies of cross sections at LHC energies thus have the potential to reveal differences from pure SM QCD, such as the presence of color-octet fermions, provided the LHC measurements are supplemented by a robust program to reduce uncertainties in α_s, PDFs, and other SM parameters, which may otherwise reduce sensitivity of the LHC observables to the gluino contributions.

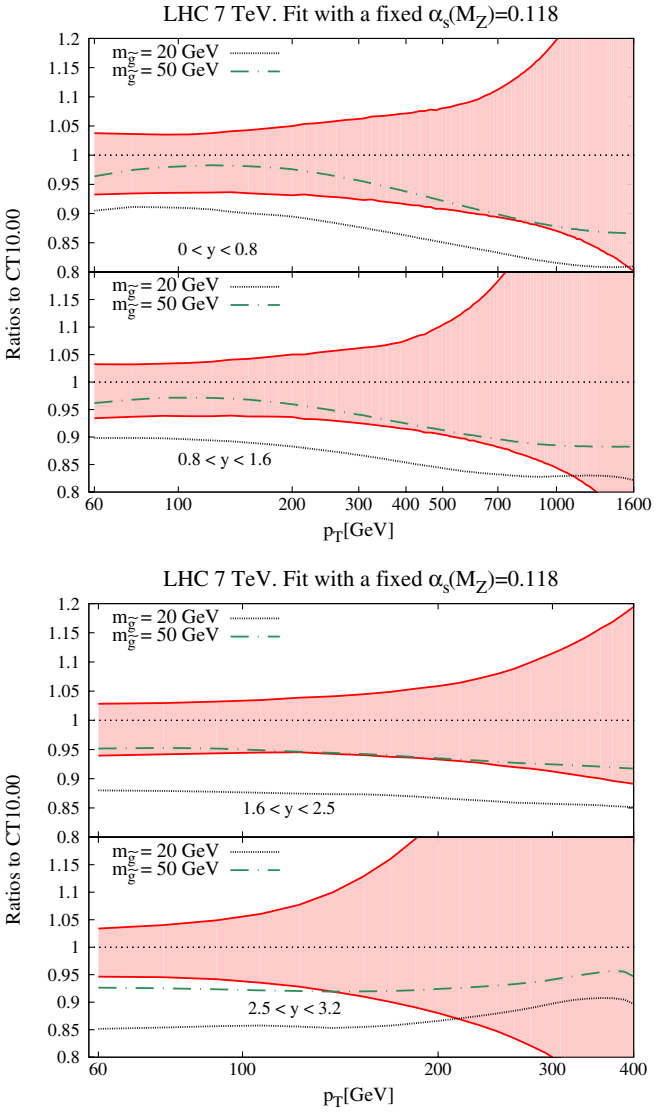

FIG. 10 (color online). Ratios of single-inclusive jet cross sections at $\sqrt{s} = 7$ TeV, obtained from the central PDF set of CT10, CT10.00, and the SM+SUSY PDFs for gluino masses $m_{\tilde{g}} = 20$ GeV (dashed line) and 50 GeV (dot-dashed line). The asymmetric PDF uncertainty of the CT10 set is also shown as a filled band. The SM+SUSY PDFs are obtained under the assumption of $\alpha_s(M_Z) = 0.118$ for both sets.

Compare, for example, single-inclusive jet cross sections at the LHC energies $\sqrt{s} = 7$ and $\sqrt{s} = 14$ TeV, computed at NLO with the Ellis-Kunszt-Soper code named EKS [45,46] in the pure SM case and in the presence of light gluinos. The CT10 asymmetric PDF error bands on the cross sections, normalized to the predictions based on the central CT10.00 PDF set, are also shown in Figs. 10–13 as a function of the jet's transverse momentum p_T, in several bins of the jet rapidity y. Ratios of the expectations based on the SM+SUSY PDFs for $m_{\tilde{g}} = 20$ and 50 GeV to their counterparts based on the CT10.00 set are shown as the dashed and dot-dashed lines, respectively.

In Figs. 10 and 11, these ratios are computed with $\alpha_s(M_Z) = 0.118$ assumed in all PDFs and cross sections. In this case, the SM+SUSY curves lie outside the respective CT10 PDF uncertainty bands for some p_T, suggesting that the SM and SM+SUSY scenarios can be distinguished, if sufficient experimental accuracy is achieved. On the other

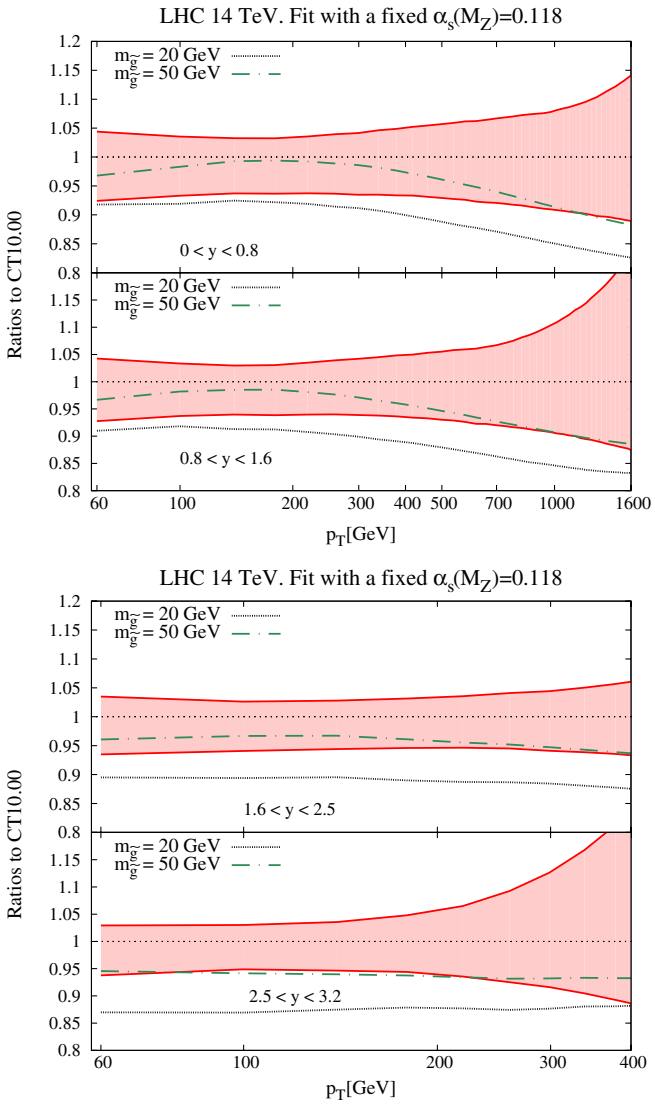

FIG. 11 (color online). Same as Fig. 10, for $\sqrt{s} = 14$ TeV.

hand, if $\alpha_s(M_Z)$ takes the values of 0.126 and 0.121 that are preferred in the SM+SUSY fits with $m_{\tilde{g}} = 20$ and 50 GeV, respectively, then the SM+SUSY curves lie within the CT10 PDF error bands, as shown in Figs. 12 and 13. In this case, discrimination of the SM and the SM+SUSY cases is more challenging, as reduction of the experimental uncertainty below the current PDF uncertainty would be necessary.

For the inclusive jet cross sections to provide a good discrimination between the SM and SM+SUSY scenarios, the uncertainties on both α_s and PDFs must be reduced below the current values. NNLO contributions to SM processes and NLO gluino contributions must also be implemented in both the PDFs and jet cross sections.

A different approach to detecting the presence of new colored states could be based on the expectation that QCD

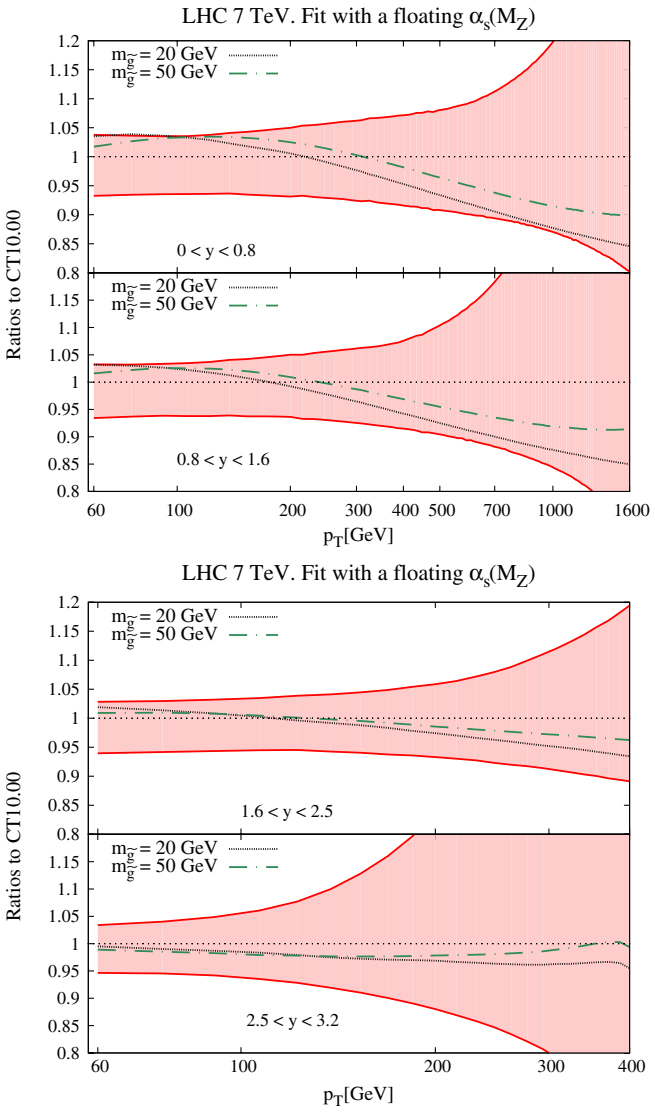

FIG. 12 (color online). Same as Fig. 10, but with $\alpha_s(M_Z) = 0.126$ in the SM+SUSY calculation with $m_{\tilde{g}} = 20$ GeV, and $\alpha_s(M_Z) = 0.121$ in the SM+SUSY calculation with $m_{\tilde{g}} = 50$ GeV.

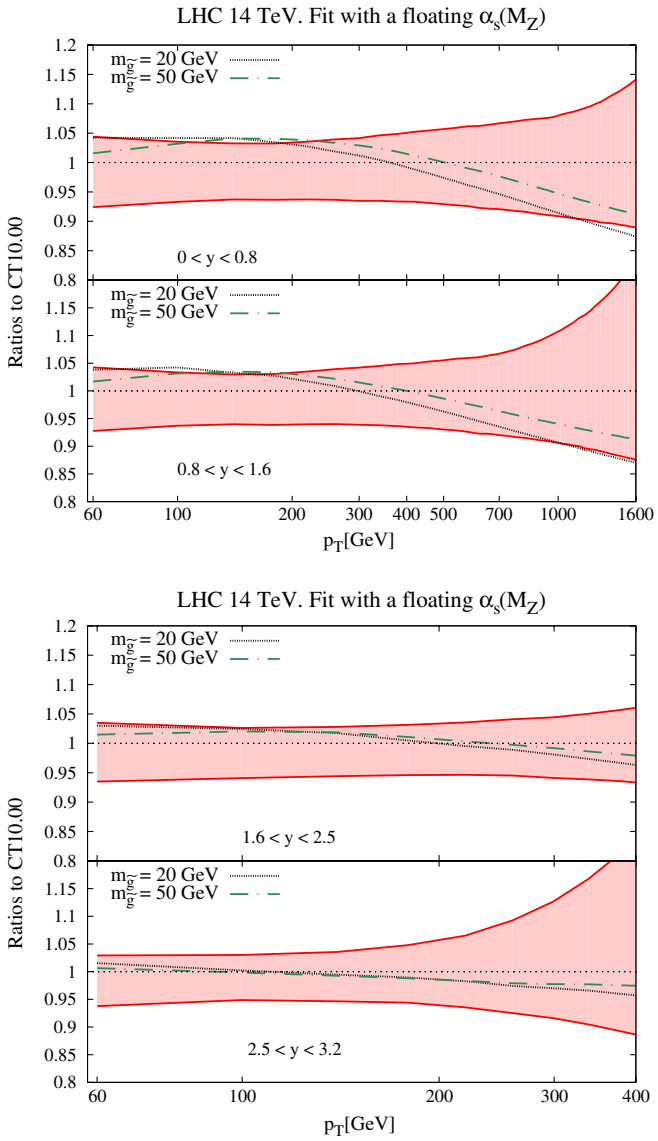

FIG. 13 (color online). Same as Fig. 12, for $\sqrt{s} = 14$ TeV.

radiation off a heavy colored object differs from that from massless partons that dominate the inclusive cross sections. It may be possible to identify jets containing gluinos by studying distributions in the jet mass or other jet shapes. The distribution in the jet mass produced by conventional QCD radiation decreases smoothly as the jet mass increases. Decays of gluinos would result in jets whose mass distributions peak at $m_{\tilde{g}}$, and gluino jet contributions could be identifiable above the continuous SM background in the distributions in the jet mass or related observables, using methods being developed [47–50].

VII. SUMMARY AND DISCUSSION

In this paper, we explore modifications in QCD scattering cross sections introduced by color-octet Majorana fermions in supersymmetry (gluinos) and other popular

extensions of the standard model. Their influence must be included in the evolution of the strong coupling strength and the parton distribution functions, especially if these fermions have mass below 100 GeV (possible in the absence of model-specific assumptions). In addition to modifying the evolution of $\alpha_s(Q)$ and the PDFs of the SM quarks and gluons, a relatively light gluino also introduces new production channels such as $gg \to \tilde{g}\,\tilde{g}$ in the inclusive jet production case. In this context, hadronic scattering data included in global PDF analyses can provide model-independent constraints on the color-octet particles.

We examine the values of χ^2 obtained from our global fits as a function of the gluino mass $m_{\tilde{g}}$. By analyzing a combination of the latest HERA and Tevatron data on hadronic scattering, and world measurements of the QCD coupling at $Q < 10$ GeV and $Q = M_Z$, we conclude that gluinos must be heavier than 25 GeV at 90% C.L., if $\alpha_s(M_Z) = 0.118$, and heavier than 15 GeV if $\alpha_s(M_Z)$ is arbitrary. These constraints supersede the 2004 study based on the CTEQ6 data set, in which we found a lower limit on the gluino mass of $m_{\tilde{g}} > 12$ GeV for $\alpha_s(M_Z) = 0.118$, and no limit if $\alpha_s(M_Z)$ is arbitrary [23]. These new bounds are comparable to the gluino mass bounds $m_{\tilde{g}} > 26.9$ and 51 GeV obtained from the analysis of event shapes in e^+e^- hadroproduction at LEP [16,17]. Our constraints on $m_{\tilde{g}}$ are obtained from the analysis of inclusive QCD observables and are not affected by theoretical uncertainties of the kind that arise in the determination of $\alpha_s(M_Z)$ from the LEP data [18–22] and LEP event shapes.

The changes in $\alpha_s(M_Z)$ and in the PDFs of standard model partons must be taken into consideration when QCD tests are made with LHC data. The high energy of the LHC and the extended range in jet transverse momentum offers hope that BSM deviations from pure QCD will show up in inclusive jet cross sections. As discussed in our comparisons with Tevatron jet data, it will be critical to control experimental uncertainties on the jet energy scale and jet energy resolution. Gluino contributions and adjustments in the SM parameters tend to offset one another. The power of precise measurements of the LHC single-inclusive jet cross sections will be enhanced provided that $\alpha_s(M_Z)$ and the PDFs for gluons and quarks are constrained more tightly than now by measurements in other channels.

For the purpose of studying jet properties in detail, we provide routines to interface with the SM+gluino PDFs. These are linked from the CTEQ webpage at cteq.org. We also note that the MADGRAPH/MADEVENT programs [51] provide a mechanism to incorporate SUSY PDFs in the initial state; information for using this interface is also provided on the webpage.

ACKNOWLEDGMENTS

We thank Tom Rizzo for discussions regarding searches for new physics and bounds on gluino masses, and Mike Whalley and Andy Buckley for extending the LHAPDF library [55,56] to incorporate PDFs with light gluinos. The authors also thank CTEQ members for helpful discussions. E. L. B. is supported by the U.S. Department of Energy under Contract No. DE-AC02-06CH11357. The work at SMU is supported in part by U.S. D.O.E. Contract No. DE-FG02-04ER41299; the U.S. D.O.E. Early Career Research Grant No. DE-SC0003870; the U.S. National Science Foundation Grant No. PHY-0705862; and by Lightner-Sams Foundation. H.-L. L. is supported by the U.S. National Science Foundation under Grant No. PHY-0855561 and by National Science Council of Taiwan under Grants No. NSC-98-2112-M-133-002-MY3 and No. NSC-99-2918-I-133-001. E. L. B. and P. M. N. thank the Aspen Center for Physics for hospitality during the summer of 2010 when part of this work was done. F. I. O thanks CERN for hospitality during his work on this study.

APPENDIX A: MODIFICATION OF THE STRONG COUPLING

The running of $\alpha_s(Q)$ must be matched to the individual PDF set with the appropriate mass thresholds. The expansion of the evolution equation for $\alpha_s(Q)$,

$$Q\frac{\partial}{\partial Q}\alpha_s(Q) = -\frac{\alpha_s^2}{2\pi}\sum_{n=0}^{\infty}\beta_n\left(\frac{\alpha_s}{4\pi}\right)^n = -\left[\beta_0\frac{\alpha_s^2}{2\pi} + \beta_1\frac{\alpha_s^3}{2^3\pi^2} + \ldots\right], \quad \text{(A1)}$$

can be solved perturbatively. It takes the form [52]

$$\alpha_s(Q) = \frac{4\pi}{\beta_0\ln(\frac{Q^2}{\Lambda^2})}\left[1 - \frac{\beta_1}{\beta_0^2}\frac{\ln[\ln(Q^2/\Lambda^2)]}{\ln(Q^2/\Lambda^2)} + \frac{\beta_1^2}{\beta_0^4\ln^2(Q^2/\Lambda^2)} + \cdots\right]. \quad \text{(A2)}$$

The beta functions, β_0 and β_1 depend on the number of active fermions and bosons. When supersymmetric particles are included [53], the first two coefficients in Eq. (A2) are

$$\beta_0 = 11 - \tfrac{2}{3}n_f - 2n_{\tilde{g}} - \tfrac{1}{6}n_{\tilde{f}},$$

and

$$\beta_1 = 102 - \tfrac{38}{3}n_f - 48n_{\tilde{g}} - \tfrac{11}{3}n_{\tilde{f}} + \tfrac{13}{3}n_{\tilde{g}}n_{\tilde{f}}, \quad \text{(A3)}$$

where n_f is the number of quark flavors, $n_{\tilde{g}}$ is the number of gluinos, and $n_{\tilde{f}}$ is the number of squark flavors. As the evolution proceeds across mass thresholds, these numbers and, consequently α_s, must be adjusted.

APPENDIX B: GLUINO CONTRIBUTIONS TO THE SINGLE-INCLUSIVE JET CROSS SECTION

The leading-order cross section for inclusive (di)jet production, $H_1H_2 \to j(p_3)j(p_4)X$, expressed in terms of the transverse momentum p_T and rapidities y_3, y_4 of the jets, is

$$\frac{d\sigma}{dp_T dy_3 dy_4} = \frac{2\pi\alpha_s^2 p_T}{\hat{s}^2}\sum_{i,j} x_1 x_2 f_{H_1\to i}(x_1,\mu_F^2) \times f_{H_2\to j}(x_2,\mu_F^2)\sum_{\text{spin}}|\mathcal{M}_{p_1p_2\to p_3p_4}|^2, \quad \text{(B1)}$$

where $x_1 = m_T/\sqrt{s}(e^{y_3}+e^{y_4})$, and $x_2 = m_T/\sqrt{s}(e^{-y_3}+e^{-y_4})$ are the parton momentum fractions, $m_T^2 = p_T^2 + m_{\tilde{g}}^2$ is the gluino's transverse mass, and $\sqrt{s}$ is the collider center-of-mass energy. In our analysis, scattering amplitudes for subprocesses with gluino pair production, $gg \to \tilde{g}\,\tilde{g}$ and $q\bar{q} \to \tilde{g}\,\tilde{g}$, are included with full dependence on gluino mass $m_{\tilde{g}}$. Scattering amplitudes for the other LO subprocesses (with at least one initial-state gluino) are evaluated in the $m_{\tilde{g}} = 0$ approximation, in accord with the S-ACOT factorization scheme [34,35].

SUSY contributions with full mass dependence can be found in the literature (e.g., in [37,54]), but they are presented here in a consistent notation for completeness. In terms of the usual parton-level Mandelstam variables, $\hat{s} = (p_1+p_2)^2$, $\hat{t} = (p_1-p_3)^2$, and $\hat{u} = (p_1-p_4)^2$, the square of the amplitude for $q\bar{q} \to \tilde{g}\,\tilde{g}$ is

$$|\mathcal{M}_{q\bar{q}\to\tilde{g}\,\tilde{g}}|^2 = \frac{8}{9}\Bigg[\frac{\hat{s}m_{\tilde{g}}^2}{3(m_{\tilde{q}}^2-\hat{t})(m_{\tilde{q}}^2-\hat{u})} + \frac{4(m_{\tilde{g}}^2-\hat{t})^2}{3(m_{\tilde{q}}^2-\hat{t})^2} - \frac{3(\hat{s}m_{\tilde{g}}^2+(m_{\tilde{g}}^2-\hat{t})^2)}{\hat{s}(m_{\tilde{q}}^2-\hat{t})} + \frac{4(m_{\tilde{g}}^2-\hat{u})^2}{3(m_{\tilde{q}}^2-\hat{u})^2} - \frac{3(\hat{s}m_{\tilde{g}}^2+(m_{\tilde{g}}^2-\hat{u})^2)}{\hat{s}(m_{\tilde{q}}^2-\hat{u})} + \frac{3(2\hat{s}m_{\tilde{g}}^2+(m_{\tilde{g}}^2-\hat{t})^2+(m_{\tilde{g}}^2-\hat{u})^2)}{\hat{s}^2}\Bigg]. \quad \text{(B2)}$$

Here $m_{\tilde{q}}$ is the mass of the squark, and the prefactor $8/9$ is a color factor. We report the expression with all the fermion mass dependence, but in our computations we have taken the limit $m_{\tilde{q}} \to \infty$.

The square of the amplitude for $gg \to \tilde{g}\,\tilde{g}$ is

$$|\mathcal{M}_{gg\to\tilde{g}\,\tilde{g}}|^2 = -\frac{9m_{\tilde{g}}^6}{4\hat{s}^2(\hat{t}-m_{\tilde{g}}^2)} - \frac{9m_{\tilde{g}}^6}{4\hat{s}^2(\hat{u}-m_{\tilde{g}}^2)} + \frac{27\hat{u}m_{\tilde{g}}^4}{4\hat{s}^2(\hat{t}-m_{\tilde{g}}^2)} - \frac{45m_{\tilde{g}}^4}{2\hat{s}(\hat{t}-m_{\tilde{g}}^2)} + \frac{27\hat{t}m_{\tilde{g}}^4}{4\hat{s}^2(\hat{u}-m_{\tilde{g}}^2)} - \frac{45m_{\tilde{g}}^4}{2\hat{s}(\hat{u}-m_{\tilde{g}}^2)} + \frac{27m_{\tilde{g}}^4}{(\hat{t}-m_{\tilde{g}}^2)(\hat{u}-m_{\tilde{g}}^2)} + \frac{9m_{\tilde{g}}^4}{\hat{s}^2} - \frac{81m_{\tilde{g}}^4}{(\hat{t}-m_{\tilde{g}}^2)^2} - \frac{81m_{\tilde{g}}^4}{(\hat{u}-m_{\tilde{g}}^2)^2} - \frac{27\hat{u}^2m_{\tilde{g}}^2}{4\hat{s}^2(\hat{t}-m_{\tilde{g}}^2)} - \frac{9\hat{t}m_{\tilde{g}}^2}{\hat{s}^2} + \frac{45\hat{u}m_{\tilde{g}}^2}{2\hat{s}(\hat{t}-m_{\tilde{g}}^2)} - \frac{9\hat{u}m_{\tilde{g}}^2}{\hat{s}^2} + \frac{9m_{\tilde{g}}^2}{\hat{s}} - \frac{27\hat{t}^2m_{\tilde{g}}^2}{4\hat{s}^2(\hat{u}-m_{\tilde{g}}^2)} + \frac{45\hat{t}m_{\tilde{g}}^2}{2\hat{s}(\hat{u}-m_{\tilde{g}}^2)} + \frac{9\hat{t}^2}{4\hat{s}^2} + \frac{9\hat{u}^2}{4\hat{s}^2} + \frac{9\hat{t}\,\hat{u}}{2\hat{s}^2} + \frac{9\hat{u}^3}{4\hat{s}^2(\hat{t}-m_{\tilde{g}}^2)} + \frac{9\hat{t}^3}{4\hat{s}^2(\hat{u}-m_{\tilde{g}}^2)}. \quad \text{(B3)}$$

APPENDIX C: PARTON LUMINOSITIES

Parton-parton luminosity functions portray the relative size of various partonic contributions. The parton luminosity is defined as a convolution integral of the PDFs $f_i(\xi,Q)$ for two incoming partons ($i,j = \tilde{g}, g, u, d, s, \ldots$):

$$\frac{d\mathcal{L}_{ij}(\tau,Q)}{d\tau} = f_i \otimes f_j = \int_\tau^1 \frac{d\xi}{\xi} f_i(\xi,Q) f_j\left(\frac{\tau}{\xi},Q\right),$$

where $\tau = \hat{s}/s$. Here $\hat{s}$ is the square of the center-of-mass energy in the incident parton-parton system. In terms of this luminosity, the production cross section for a specific reaction is

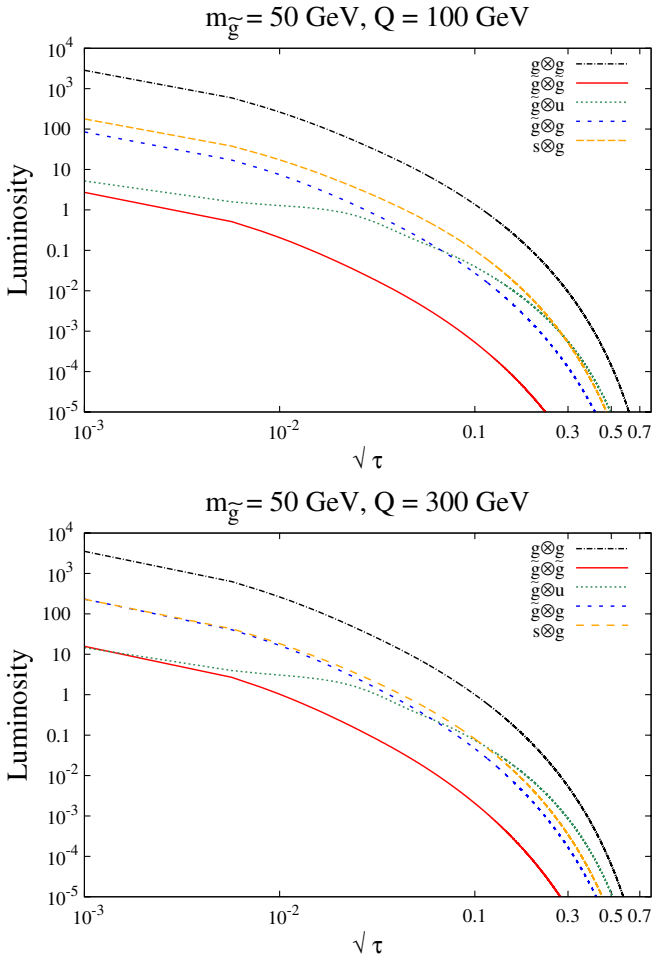

FIG. 14 (color online). Parton-parton luminosity $\tau d\mathcal{L}_{ij}(\tau,Q)/d\tau$ vs $\sqrt{\tau}$ for $m_{\tilde{g}} = 50$ GeV at $Q = 100$ and 300 GeV.

$$\sigma(s) = \sum_{i,j} \int_{\tau_0}^{1} d\tau \hat{\sigma}_{ij}(\tau) \frac{d\mathcal{L}_{ij}(\tau, Q)}{d\tau}. \quad \text{(C1)}$$

The sum is over the initial-state parton flavors i and j, and $\hat{\sigma}_{ij}(\tau)$ is the partonic cross section for the subprocess initiated by partons i, j.

The luminosities for some flavor combinations are shown in Fig. 14 for $m_{\tilde{g}} = 50$ GeV. At $Q = 100$ GeV all gluino luminosities are smaller than the SM luminosities, but they grow in magnitude as Q increases. The gluon-gluino luminosity is roughly the same as the gluon-bottom quark luminosity, as would be expected from the momentum fractions presented in Table I. At $Q = 300$ GeV the $\tilde{g} \otimes g$ contribution is comparable to that of the ordinary quarks. The $\tilde{g} \otimes g$ combination is smaller than $s \otimes g$ throughout the x range for $Q = 100$ GeV. At $Q = 300$ GeV, the evolution of the gluino is enhanced, and $\tilde{g} \otimes g$ exceeds various SM pairings for $x > 0.1$.

[1] H. E. Haber and G. L. Kane, Phys. Rep. **117**, 75 (1985).
[2] T. Appelquist, H.-C. Cheng, and B. A. Dobrescu, Phys. Rev. D **64**, 035002 (2001).
[3] L. Randall and R. Sundrum, Phys. Rev. Lett. **83**, 3370 (1999).
[4] N. Arkani-Hamed, A. G. Cohen, and H. Georgi, Phys. Lett. B **513**, 232 (2001).
[5] J. Alitti *et al.* (UA2 Collaboration), Phys. Lett. B **235**, 363 (1990).
[6] V. M. Abazov *et al.* (D0 Collaboration), Phys. Lett. B **638**, 119 (2006).
[7] V. M. Abazov *et al.* (D0 Collaboration), Phys. Rev. Lett. **99**, 131801 (2007).
[8] V. M. Abazov *et al.* (D0 Collaboration), Phys. Lett. B **660**, 449 (2008).
[9] V. M. Abazov *et al.* (D0 Collaboration), Phys. Lett. B **680**, 24 (2009).
[10] T. Aaltonen *et al.* (CDF Collaboration), Phys. Rev. Lett. **102**, 221801 (2009).
[11] T. Aaltonen *et al.* (CDF Collaboration), Phys. Rev. Lett. **102**, 121801 (2009).
[12] A. Abulencia *et al.* (CDF Collaboration), Phys. Rev. Lett. **96**, 171802 (2006).
[13] A. Abulencia *et al.* (CDF Collaboration), Phys. Rev. Lett. **97**, 171802 (2006).
[14] J. Alwall, M.-P. Le, M. Lisanti, and J. G. Wacker, Phys. Lett. B **666**, 34 (2008).
[15] C. F. Berger, J. S. Gainer, J. L. Hewett, and T. G. Rizzo, J. High Energy Phys. 02 (2009) 023.
[16] A. Heister *et al.* (ALEPH Collaboration), Eur. Phys. J. C **31**, 327 (2003).
[17] D. E. Kaplan and M. D. Schwartz, Phys. Rev. Lett. **101**, 022002 (2008).
[18] T. Becher and M. D. Schwartz, J. High Energy Phys. 07 (2008) 034.
[19] R. A. Davison and B. R. Webber, Eur. Phys. J. C **59**, 13 (2009).
[20] G. Dissertori *et al.*, J. High Energy Phys. 08 (2009) 036.
[21] R. Abbate, M. Fickinger, A. Hoang, V. Mateu, and I. W. Stewart, Proc. Sci. RADCOR2009 (**2010**) 040.
[22] R. Abbate, M. Fickinger, A. H. Hoang, V. Mateu, and I. W. Stewart, arXiv:1006.3080.
[23] E. L. Berger, P. M. Nadolsky, F. I. Olness, and J. Pumplin, Phys. Rev. D **71**, 014007 (2005).
[24] H.-L. Lai, M. Guzzi, J. Huston, Z. Li, P. M. Nadolsky, J. Pumplin, and C.-P. Yuan, Phys. Rev. D **82**, 074024 (2010).
[25] H.-L. Lai *et al.*, Phys. Rev. D **82**, 054021 (2010).
[26] T. Aaltonen *et al.* (CDF Collaboration), Phys. Rev. D **78**, 052006 (2008).
[27] A. Abulencia *et al.* (CDF Collaboration), Phys. Rev. D **75**, 092006 (2007).
[28] V. M. Abazov *et al.* (D0 Collaboration), Phys. Rev. Lett. **101**, 062001 (2008).
[29] F. D. Aaron *et al.* (H1 Collaboration and ZEUS Collaboration), J. High Energy Phys. 01 (2010) 109.
[30] V. M. Abazov *et al.* (D0 Collaboration), Phys. Rev. D **80**, 111107 (2009).
[31] N. Arkani-Hamed and S. Dimopoulos, J. High Energy Phys. 06 (2005) 073.
[32] G. F. Giudice and A. Romanino, Nucl. Phys. **B699**, 65 (2004).
[33] E. L. Berger, B. Harris, D. Kaplan, Z. Sullivan, T. M. Tait, and C. Wagner, Phys. Rev. Lett. **86**, 4231 (2001).
[34] J. C. Collins, Phys. Rev. D **58**, 094002 (1998).
[35] M. Kramer, F. I. Olness, and D. E. Soper, Phys. Rev. D **62**, 096007 (2000).
[36] P. A. Baikov, K. G. Chetyrkin, and J. H. Kuhn, Phys. Rev. Lett. **101**, 012002 (2008).
[37] C. Amsler *et al.* (Particle Data Group), Phys. Lett. B **667**, 1 (2008).
[38] LEP (LEP, ALEPH, DELPHI, L3, OPAL, LEP Electroweak Working Group, and SLD Collaborations), arXiv:hep-ex/0312023.
[39] J. Pumplin, D. Stump, J. Huston, H. Lai, P. M. Nadolsky, and W. Tung, J. High Energy Phys. 07 (2002) 012.
[40] P. M. Nadolsky *et al.*, Phys. Rev. D **78**, 013004 (2008).
[41] P. M. Nadolsky and Z. Sullivan, in *Proceedings of the APS / DPF / DPB Summer Study on the Future of Particle Physics, Snowmass, Colorado, 2001)* econf C010630, P510 (unpublished), arXiv:hep-ph/0110378 .
[42] A. A. Affolder *et al.* (CDF Collaboration), Phys. Rev. D **64**, 032001 (2001).
[43] B. Abbott *et al.* (D0 Collaboration), Phys. Rev. D **64**, 032003 (2001).
[44] J. Pumplin, J. Huston, H. L. Lai, W.-K. Tung, and C.-P. Yuan, Phys. Rev. D **80**, 014019 (2009).
[45] S. D. Ellis, Z. Kunszt, and D. E. Soper, Phys. Rev. Lett. **64**, 2121 (1990).

[46] S. D. Ellis, Z. Kunszt, and D. E. Soper, Phys. Rev. Lett. **69**, 1496 (1992).
[47] J. Thaler and L.-T. Wang, J. High Energy Phys. 07 (2008) 092.
[48] L. G. Almeida, S. J. Lee, G. Perez, I. Sung, and J. Virzi, Phys. Rev. D **79**, 074012 (2009).
[49] L. G. Almeida *et al.*, Phys. Rev. D **79**, 074017 (2009).
[50] S. D. Ellis, C. K. Vermilion, and J. R. Walsh, Phys. Rev. D **80**, 051501 (2009).
[51] J. Alwall *et al.*, J. High Energy Phys. 09 (2007) 028.
[52] W. M. Yao *et al.* (Particle Data Group), J. Phys. G **33**, 1 (2006).
[53] M. E. Machacek and M. T. Vaughn, Nucl. Phys. **B222**, 83 (1983).
[54] W. Beenakker, R. Hopker, M. Spira, and P. M. Zerwas, Nucl. Phys. **B492**, 51 (1997).
[55] D. Bourilkov, R. C. Group, and M. R. Whalley, arXiv:hep-ph/0605240.
[56] M. R. Whalley, D. Bourilkov, and R. C. Group, arXiv:hep-ph/0508110.7